This article has been accepted for publication in a future issue of this journal, but has not been fully edited. Content may change prior to final publication. Citation information: DOI 10.1109/TBCAS.2021.3087475, IEEE Transactions on Biomedical Circuits and Systems

A Portable Wireless Urine Detection System with Power-Efficient Electrochemical Readout ASIC and ABTS-CNT Biosensor for UACR Detection

Shuenn-Yuh Lee, *Senior Member*, *IEEE*, Hao-Yun Lee, *Student Member*, *IEEE*, Ding-Siang Ciou, Zhan-Xian Liao, *Student Member*, *IEEE*, Peng-Wei Huang, Yi-Ting Hsieh, Yi-Chieh Wei, Chia-Yu Lin, Meng-Dar Shieh, and Ju-Yi Chen

***Abstract* — This work presents a portable wireless urine detection system which consists of an electrochemical readout application specific integrated circuit (ASIC) and a biosensor composed of 2,2'-azino-bis(3-ethylbenzothiazoline-6-sulphonic acid) and carbon nanotube (ABTS-CNT) for the detection of urine albumin-to-creatinine ratio (UACR). The ASIC includes a potentiostat, a digital circuitry and a power management circuit which can perform electrochemistry techniques with a dual-channel screen-printing carbon electrode (SPCE). Electrochemical experiments on the proposed biosensor (SPCE|ABTS-CNT|Nafion®) have revealed promising sensing characteristics for creatinine and human serum albumin detection. Practical urine tests has demonstrated the capability of the proposed urine detection system for UACR detection with both the power-efficient readout ASIC and the ABTS-CNT biosensor. A user-friendly prototype has also been designed which can be useful for either personal health administration or homecare.**

Keywords: current readout circuit, VCO-based continuous-time delta-sigma modulator, screen-printed carbon electrode, urine detection system, electrochemistry acquisition, urine albumin-to-creatinine ratio.

I. Introduction

Owing to the increasing stress in modern society and the irregular lifestyle, cardiovascular diseases have become a serious health concern with a high mortality rate worldwide. According to a recent survey by the World Health Organization (WHO) [1], cardiovascular diseases account for over 31% of all global deaths in 2016, and an estimated 17.9 million people died from such diseases. To address these problems, the WHO suggested that among the keys to successful treatment and prevention of such diseases is the early detection. Several cardiovascular diseases, such as hyperlipidemia, hypertension, and heart failure, can be prevented by detecting the risk factors highly associated with these diseases, especially some specific biomarkers in body fluids. Therefore, a reliable detection system and a platform for the rapid test of cardiovascular risk factors must be developed. Such a system can be popularized by ensuring the preventive assessment is user-friendly. However, the diagnosis of cardiovascular diseases is conventionally confirmed by blood examination, which is an invasive procedure because it involves collecting blood samples. Such an invasive method is usually inconvenient and time-consuming which may dramatically delay the assessment of risk factors for the early detection. Detecting these risk factors from urine is an emerging candidate for noninvasive diagnosis. In previous medical studies, several important biomarkers in urine has been focused, such as the creatinine and albumin [2]. These two biomarkers usually form the urine albumin-to-creatinine ratio (UACR), which is a well-known urinary index for examining kidney functions and cardiovascular diseases. Creatinine is the by-product of the spontaneous dehydration of muscle creatine and the dephosphorylation of creatine phosphate in muscle metabolism. The concentration of creatinine in healthy human serum and urine ranges from 40 μM to 150 μM [3] and 5.92 mM to 19.01 mM [4], respectively. As it is excreted by glomerular filtration at a relatively constant rate, urine creatinine is used not only as an important index of renal glomerular filtration rate but also as an internal standard for testing urine adulteration and normalizing urinary biomarkers, such as albumin. Human serum albumin (HSA) is the most abundant protein in blood serum. The concentration of HSA is regarded as an indicator of presence of

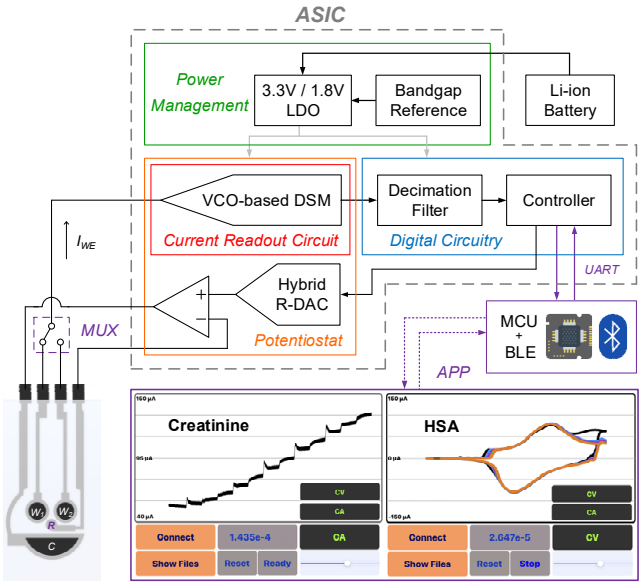

Fig. 1. Block diagram of the proposed urine detection system which includes an electrochemical readout ASIC and a dual-channel biosensor.

This research was supported in part by the Taiwan Semiconductor Research Institute and the Ministry of Science and Technology (MOST), Taiwan, R.O.C., under Grants MOST 109-2218-E-006-022 and MOST 109-2622-8-006-021-TE2 (*Corresponding author: Shuenn-Yuh Lee and Ju-Yi Chen*).

S. Y. Lee, H. Y. Lee, D. S. Ciou, Z. X. Liao, P. W. Huang, and Y. T. Hsieh are with the Department of Electrical Engineering, National Cheng Kung University, Tainan 701, Taiwan (e-mail: ieesyl@mail.ncku.edu.tw, lhyjason92@gmail.com).

C. Y. Lin is with the Department of Chemical Engineering, National Cheng Kung University, Tainan 701, Taiwan (e-mail: cyl44@mail.ncku.edu.tw).

M. D. Shieh and Y. C. Wei are with the Department of Industrial Design, National Cheng Kung University, Tainan 701, Taiwan (e-mail: mdshieh@mail.ncku.edu.tw).

J. Y. Chen is with Department of Internal Medicine, National Cheng Kung University Hospital, College of Medicine, National Cheng Kung University, Tainan, 701 Taiwan (e-mail: juyi@mail.ncku.edu.tw)

This article has been accepted for publication in a future issue of this journal, but has not been fully edited. Content may change prior to final publication. Citation information: DOI 10.1109/TBCAS.2021.3087475, IEEE Transactions on Biomedical Circuits and Systems

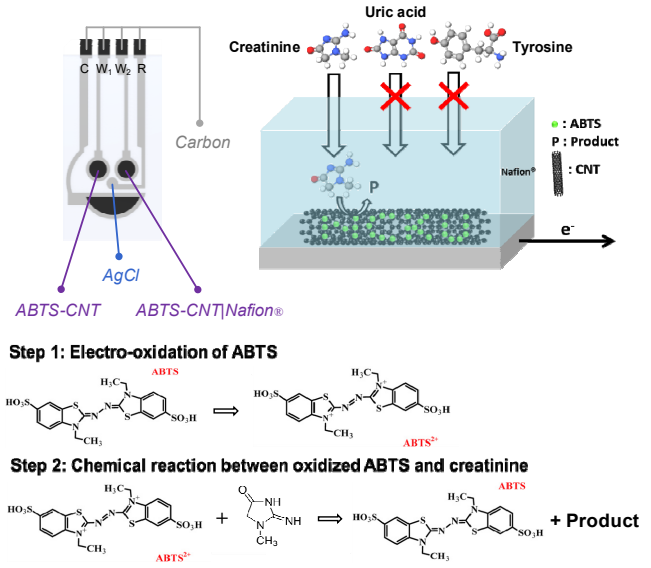

Fig. 2. Configuration of the proposed dual-channel electrochemical biosensor.

various diseases, such as cardiovascular diseases, diabetes mellitus, and kidney diseases. Hence, the quantitation of HSA in biological fluids is important for the diagnosis of these diseases. The normal HSA concentration ranges from 3.5 mg/dL to 5.0 mg/dL in the blood [5] and is less than 20 mg/dL in urine [6], respectively.

II. Proposed Electrochemical System

Electrochemistry is usually adopted in noninvasive diagnosis. Electrochemical readout circuits have attracted public attention throughout the years [7-9] as the awareness of personal health monitoring. Compared with chromatography and spectroscopy, electrochemistry acquisition has the capability of integration and rapid detection, and thus can be utilized in sensor applications. A reliable three-electrode sensor and an electrochemical readout circuit are necessary to provide redox reaction and implement an electrochemical system for the UACR detection. The block diagram of the urine detection system proposed herein is given in Fig. 1. It is composed of an electrochemical readout application specific integrated circuit (ASIC), a dual-channel biosensor, an external MCU with Bluetooth module for wireless transmission, and a smartphone application (APP) as the user interface. The readout ASIC includes a potentiostat, a digital circuitry and a power management circuit which can perform electrochemistry techniques, such as chronoamperometry (CA) and cyclic voltammetry (CV), with the dual-channel biosensor. The proposed potentiostat for three-electrode electrochemical measurements includes a current readout circuit and a waveform pattern generator that are implemented by a current-sensing voltage-controlled oscillator-based (VCO-based) continuous-time delta-sigma modulator (CTDSM) and a hybrid resistor-based digital-to-analog converter (R-DAC), respectively. The electrochemical cell is stimulated by a fixed (in CA) or a triangular (in CV) voltage waveform through the hybrid R-DAC. The redox reaction current (I_{WE}) sensed from the working electrode is directly quantized by the VCO-based CTDSM with a decimation filter for signal acquisition. The input instruction to the internal controller and the output data from the decimation filter are transmitted in a universal asynchronous receiver-

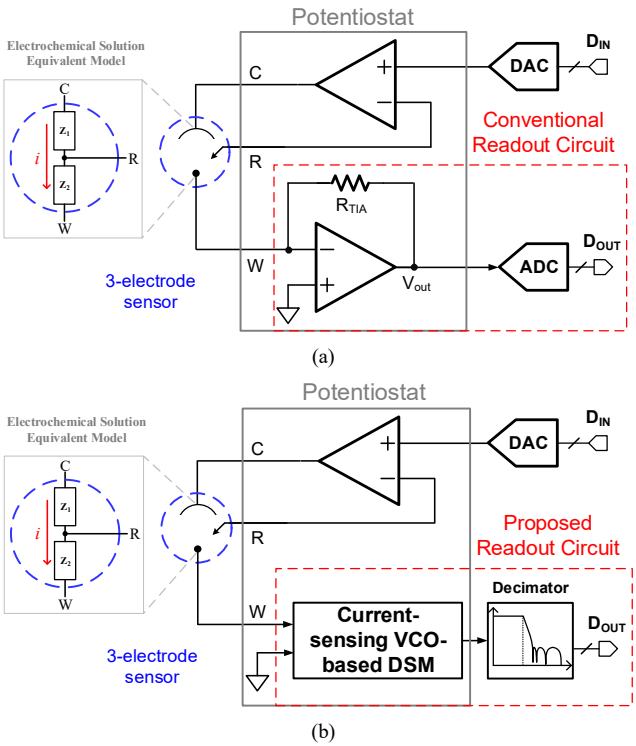

Fig. 3. (a) Conventional architecture of potentiostat with the TIA topology. (b) Proposed readout circuit with a direct connection to the sensor in potentiostat.

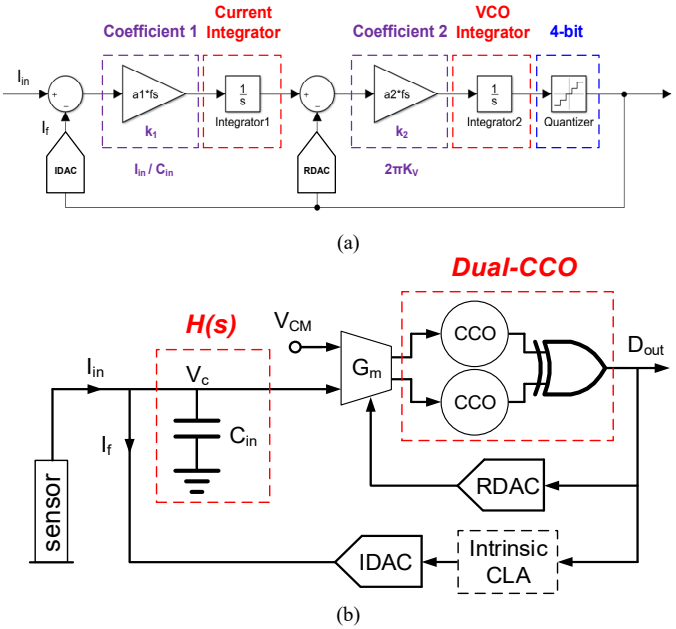

Fig. 4. (a) Topology of the current-sensing VCO-based 2nd-order CTDSM. (b) Circuit architecture of proposed VCO-based CTDSM for sensor application.

transmitter (UART) package by the signal processing of digital circuitry. Finally, the measurement result is displayed on our developed APP by the external Bluetooth module. Moreover, combined with the dual-channel electrochemical biosensor developed in our previous work [10], which consists of the composite of 2,2'-azino-bis(3-ethylbenzothiazoline-6-sulphonic acid) and carbon nanotube (ABTS-CNT), the two biomarkers

This article has been accepted for publication in a future issue of this journal, but has not been fully edited. Content may change prior to final publication. Citation information: DOI 10.1109/TBCAS.2021.3087475, IEEE Transactions on Biomedical Circuits and Systems

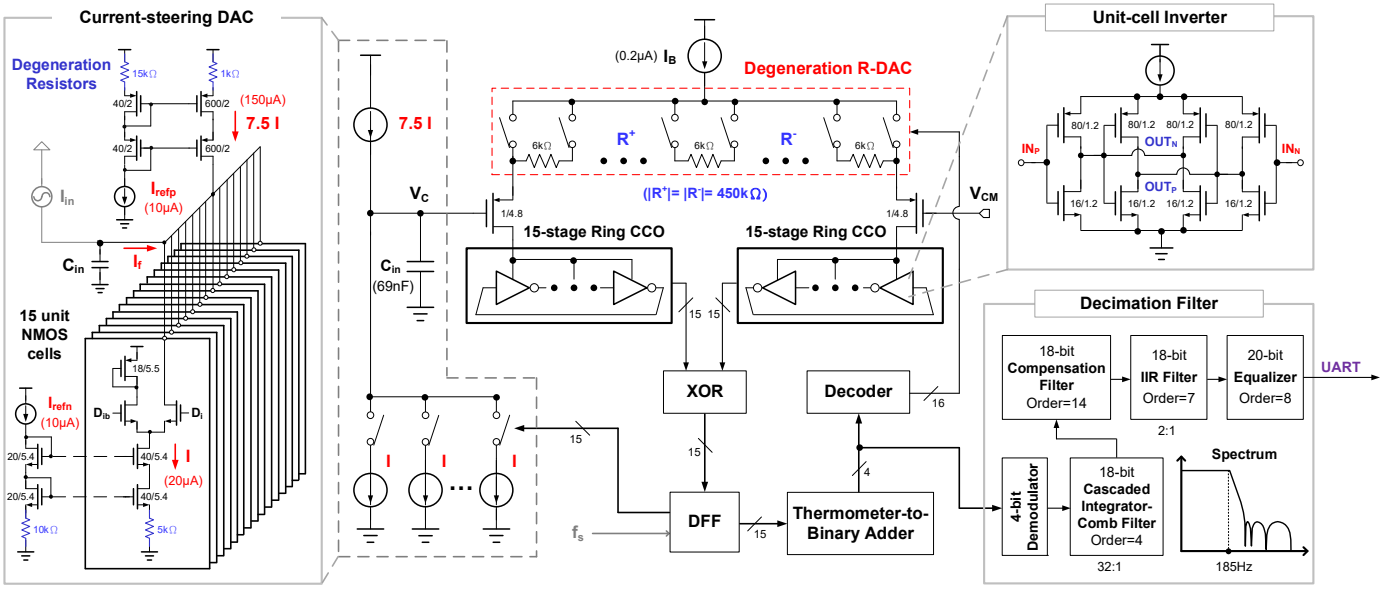

Fig. 5. Detailed structure of the proposed current-sensing VCO-based 2nd-order delta-sigma ADC.

(i.e., creatinine and albumin) can be easily and readily detected by the proposed urine detection system. Hence, this system is suitable for the noninvasive early detection of cardiovascular risk factors.

For UACR detection, an electrochemical sensor with high sensitivity and selectivity to the two urinary biomarkers (i.e., creatinine and albumin) has been developed. The configuration of the proposed electrochemical biosensor, which consists of the SPCE modified with the ABTS-CNT composite, as well as a Nafion® overlayer to minimize the interference in practical urine tests, such as uric acid and tyrosine, is provided in Fig. 2. Creatinine detection is based on the oxidation of ABTS and the subsequent chemical reaction between the ABTS radical cations ($ABTS^{2+}$) and creatinine. The two steps of the redox reaction are depicted in Fig. 2. The amperometric tests by an electrochemical analyzer (CHI 660) have revealed the promising sensing characteristics of the biosensor, including a high sensitivity of 28.08 μA cm^{-2} mM^{-1}, a wide linear range of 0–21.3 mM, a fast response time of less than 60 s, and a low limit of detection of 10.92 μM. By comparison, HSA detection is based on the SPCE modified with the ABTS-CNT dispersion solution without the addition of an Nafion® overlayer because the tyrosyl and tryptophanyl amino acid residues in HSA can be oxidized on the carbon electrode. The proposed dual-channel biosensor looks like a “smiling face”, where the two eyes are coated with the ABTS-CNT composite with and without Nafion® for the detection of creatinine and albumin respectively, and the material used for printed reference electrode (RE) on the nose is the AgCl. The counter electrode (CE) and the 4-pin connectors are all made of carbon electrodes. Owing to the different physical and electrochemical properties of the two biomarkers, different electrochemistry techniques should be applied, such as the CA for creatinine detection and the CV for HSA detection. Based on the amperometric characteristics and the area of the targeted working electrode, the peak reaction current of biosensor examined from the experiment results is about 150 μA in the CV measurement of HSA detection.

The core of the analog readout circuit is the potentiostat, which can provide redox reaction and signal acquisition. In three-electrode electrochemical measurements, the conventional approach for detecting sensor currents is to employ a trans-impedance amplifier (TIA) at the analog front end (AFE), as shown in Fig. 3(a). Although this TIA topology is straightforward in terms of circuit implementation, the use of an extra operational amplifier usually leads to higher power consumption and noise contribution. The direct current-sensing technique is considered as an alternative approach [11] in the readout circuit. In this topology, the analog-to-digital converter (ADC) must directly digitize the sensor current within a non-amplified input signal dynamic range and requires the same input-referred noise and linearity performance as that of a TIA. In this work, a current-sensing VCO-based 2nd-order CT delta-sigma ADC modified from our previous work [12] is proposed as the readout circuit in potentiostat, as shown in Fig. 3(b). Via the high DC loop gain of DSM, the voltage on the working electrode can be forced to a desired bias voltage in the closed-loop feedback network. The proposed VCO-based CTDSM features direct connection to the electrochemical biosensor without pre-amplifier, which can directly quantize the current signal from the redox reaction. Second-order noise shaping is achieved by using an additional capacitor as a passive integrator and a dual-VCO structure as a phase integrator. For sensor applications, the proposed architecture can perfectly act as an amplifier-less current readout circuit in potentiostat with a better power efficiency.

In this study, a urine detection system with a power-efficient electrochemical readout ASIC and a dual-channel biosensor is proposed for UACR detection. This paper is organized as follows. Section III describes the design details and the circuit implementation of the proposed electrochemical readout ASIC and also shows the configuration of the proposed dual-channel ABTS-CNT biosensor. Section IV presents the measured ASIC performance and the experiment results of practical urine sample tests. Finally, a brief conclusion is drawn in Section V.

This article has been accepted for publication in a future issue of this journal, but has not been fully edited. Content may change prior to final publication. Citation information: DOI 10.1109/TBCAS.2021.3087475, IEEE Transactions on Biomedical Circuits and Systems

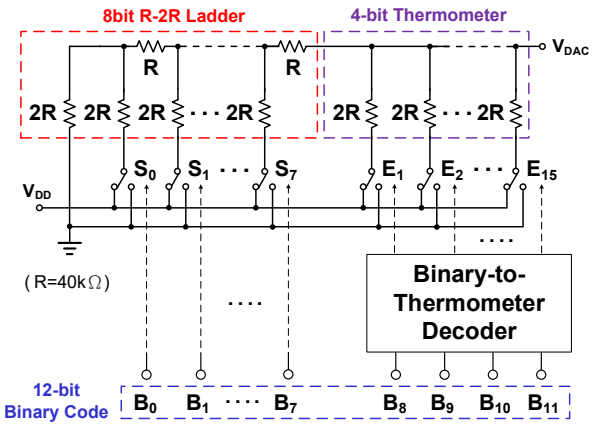

(a)

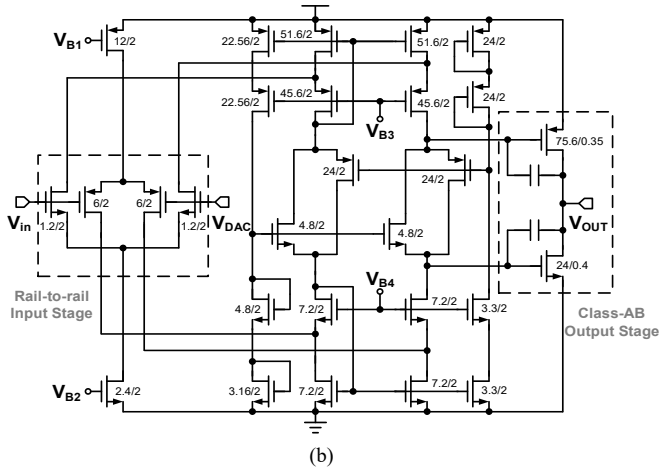

(b)

Fig. 6. (a) Architecture of the 12-bit hybrid R-DAC. (b) Schematic of the rail-to-rail amplifier with a class-AB output stage which is the one shown in the block diagram of Fig. 1 between the DAC and the biosensor.

III. Circuit Design of Proposed ASIC

A. Current-sensing VCO-based CT delta-sigma ADC

The topology of the proposed 2nd-order continuous-time low-pass DSM is shown in Fig. 4(a). It applies the multi-feedback technique and the multi-bit quantization, which adopts a current integrator and a VCO-based phase integrator to achieve second-order noise shaping. In this topology, almost all the coefficients in the loop filter are directly dependent on system specifications and hence become highly reconfigurable. The circuit architecture of the proposed VCO-based CTDSM is shown in Fig. 4(b). By applying the direct sensing technique to the electrochemical sensor instead of any pre-amplifier, the power efficiency defined in [13] can be substantially improved. The transfer functions and coefficients in the first and the second stages are expressed by the following formulas:

$$\Delta V_C = \frac{I_{in}}{sC_{in}} = \frac{a_1 f_s}{s}, \tag{1}$$

$$\frac{\Delta\varphi(s)}{\Delta V_C} = \frac{2\pi K_V}{s} = \frac{2\pi \cdot G_m}{s \cdot NC_{CCO}V_{DD\_CCO}} = \frac{a_2 f_s}{s}, \tag{2}$$

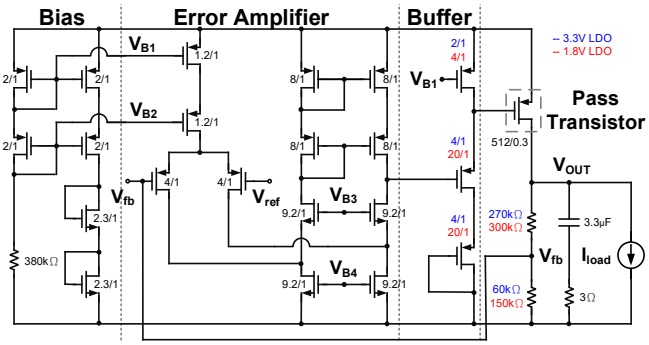

Fig. 7. Schematic of the low-dropout regulators.

Where ΔV_c is the output range on the input capacitor, I_{in} is the designed input amplitude equal to 150 μA in this work, C_{in} is a passive capacitance at AFE, $\Delta\varphi$ is the phase difference between the two G_m-CCOs, K_v is the voltage-to-frequency converter coefficient, N is the number of current controlled oscillator (CCO) stages, C_{CCO} is the parasitic capacitance in each stage of CCO, V_{DD_CCO} is the supply voltage of CCO, G_m is the effective transconductance of the input transistors in the second stage, and f_s is the sampling frequency of DSM.

According to these formulas, the proposed VCO-based current readout circuit can simply act as a 2nd-order CTSDM, the system coefficients of which are directly determined by the ratio of peak input current to passive capacitance (I_{in}/C_{in}) and the VCO tuning gain (K_v). The detailed structure of the proposed VCO-based CTDSM is presented in Fig. 5. Given that the current integrator in the first stage is achieved by charging C_{in} with the error signal (I_{in}-I_f), a current-steering DAC is required. Both large transistors and degeneration resistors are used to minimize the effects of flicker noise [14]. A dual-VCO structure acting as both the 4-bit quantizer and the phase integrator in the second stage is adopted to detect phase difference between the two G_m-$CCOs$, which can be realized as a differential pair with source degeneration, a 15-stage CCO for each branch path, and an XOR gate as the phase detector. For the negative-feedback path to the two G_m-CCOs, a degeneration R-DAC [15] is utilized to balance the branch currents and facilitate the convergence of frequency difference to zero in steady state, which only needs an extra thermometer-to-binary adder and a simple 4-to-16 decoder to ensure low power consumption. By this technique, the related parameters between the first and the second stages can be derived as

$$\frac{I_B}{2}(R^+ - R^-) = \Delta V_C = \frac{I_{in}}{sC_{in}}. \tag{3}$$

In order to keep the linearity of K_V acceptable, the ΔV_C should be small enough, which maximum value is designed as 90 mV_{pp} in this work to ensure the linearity of K_V in the second stage.

The 4-bit digital outputs of DSM are demodulated by adopting a decimation filter with the cascade structure similar to that we described in our previous work [16] for ECG signal acquisition. This structure includes a cascaded integrator-comb (CIC) filter, a compensation filter, an infinite impulse response

This article has been accepted for publication in a future issue of this journal, but has not been fully edited. Content may change prior to final publication. Citation information: DOI 10.1109/TBCAS.2021.3087475, IEEE Transactions on Biomedical Circuits and Systems

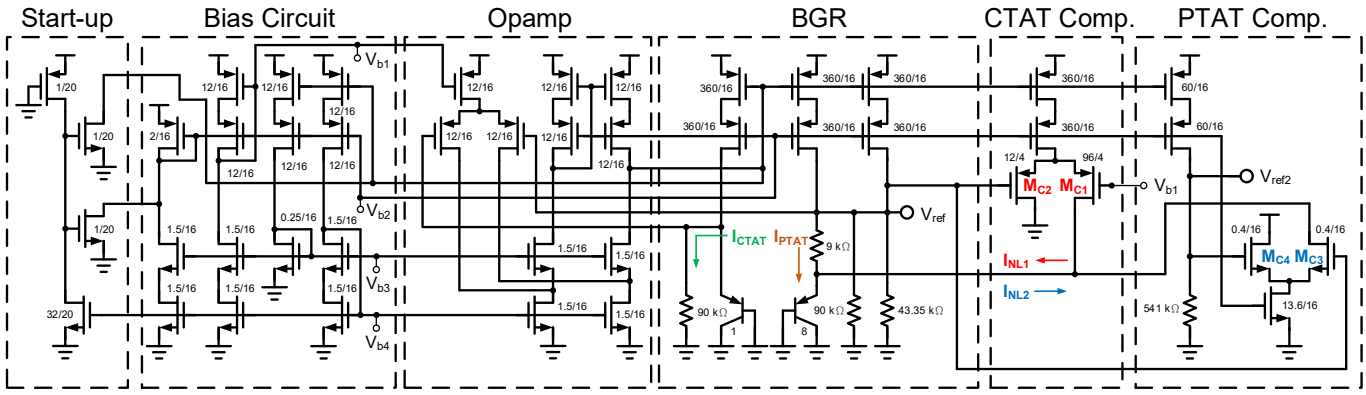

Fig. 8. Detailed circuit implementation of the proposed BGR.

(IIR) filter, and an equalizer. The 4th-order CIC filter is used to downsample the output data of DSM and extend the bit length to achieve a high decimation ratio of 32 with sufficient attenuation of stopband. The compensation filter is applied to compensate the in-band gain loss of the previous CIC filter and flatten the passband by using an equiripple finite impulse response (FIR) filter. The whole decimation ratio of 64 is completed and a sharp transition band filter is constructed using the IIR filter to achieve a decimation ratio of 2 with fewer coefficients and a shorter delay time than the FIR filter. The main problem of its nonlinear phase is solved by appending an equalizer behind to minimize variations in group delay. The output data of DSM are demodulated via the digital circuitry and filtered at a signal bandwidth of 200 Hz and finally transmitted in UART 8-N-1 format [17] via Bluetooth.

B. On-chip Waveform Generator

The electrochemical cell is stimulated by the corresponding voltage waveforms to each electrochemistry by using a pattern generator in the potentiostat designed herein, and thus an on-chip waveform generator is necessary. In this work, the circuit blocks for the pattern generator consist of a hybrid R-DAC and a class-AB amplifier as shown in the previous Fig. 1. The architecture of the 12- bit hybrid R-DAC with a 4-bit coarse segment and an 8-bit fine segment is illustrated in Fig. 6(a). The fine segment is composed of an 8-bit R-2R ladder for saving the required amounts of switches and wires, whereas the coarse segment is utilized by a 4-bit resistor-string in thermometer with a binary-to-thermometer decoder. The four MSBs of the 16-bit data word are decoded to drive 15 switches (E_1 to E_{15}), which connect one of the 15 matched resistors to either ground or V_{DD} and the remaining 8 bits of the data word drive switches (S_0 to S_7) of a voltage mode R-2R ladder network. With this structure, the maximum DNL error is alleviated via the hybrid of the resistor-string in thermometer instead of the pure R-2R ladder. For the rail-to-rail operation, a folded-cascode amplifier with class-AB output stage is implemented as the output buffer of hybrid R-DAC for the three-electrode electrochemical measurement in potentiostat (Fig. 6(b)). The main design considerations include the gain error, driving ability and stability of this opamp. According to the equivalent model of the electrochemical solution drawn in Fig. 3, the situation is like a non-inverting amplifier operation where the feedback network is composed of the unknown Z_1 and Z_2, and the output driving current is equal to

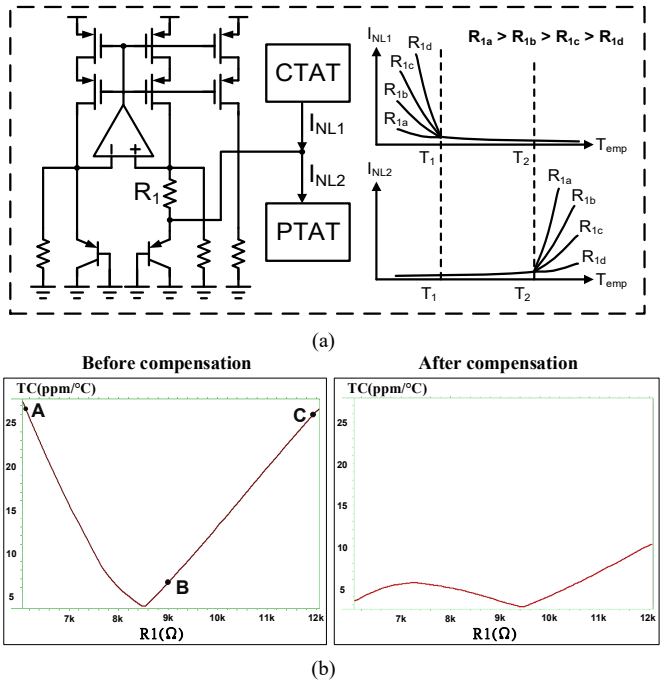

Fig. 9. (a) Operation principle of the proposed BGR compensation. (b) The simulation of TC over the resistor variation before and after compensation.

i from the redox reaction of the biosensor. Therefore, the gain error will cause a lower accuracy and can't provide a precise working potential (ΔV_{WR}). Because the feedback network is uncertain, both the output current and the phase margin should be designed large enough to ensure driving ability and stability for the sensor loading current. Under the same specification requirements, the class-AB structure can achieve a better power efficiency compared with other types of opamp, such as the conventional two-stage opamp. In this work, the DC gain is designed approximately to 100 dB with a bandwidth of 1.8 MHz, and the phase margin is designed to 73° for the stability. The output current are designed approximately to 150 μA according to the peak reaction current of biosensor examined from the experiment results.

The proposed generator can stimulate two types of waveform pattern for the working potential (ΔV_{WR}) according to the

This article has been accepted for publication in a future issue of this journal, but has not been fully edited. Content may change prior to final publication. Citation information: DOI 10.1109/TBCAS.2021.3087475, IEEE Transactions on Biomedical Circuits and Systems

different electrochemistry techniques for the two biomarkers, which are correspondingly a step of 1.05 V for CA and a triangular wave of 0–0.8 V at a sweep rate of 0.1 V/s for CV.

C. Power Management Circuit

The implemented power management circuit includes low-dropout regulators (LDOs) and a bandgap reference (BGR). The schematic of the LDOs that can provide 1.8 and 3.3 V supply voltages for the ASIC is given in Fig. 7. Quiescent current, stability, line regulation, and load regulation are the important design issues in power management circuits. The closed-loop of the LDOs consists of an error amplifier, a buffer stage that serves as the stability compensator and level shifter, a pass transistor, and two feedback resistors. The feedback network can regulate the output voltage to achieve a desired line regulation and load regulation and accordingly a clean power supply for the entire electrochemical system.

A BGR circuit is required to achieve the precise output voltage and provide V_{ref} for the LDOs. The detailed circuit implementation in transistor level of the proposed BGR that has the ability against resistor variations is depicted in Fig. 8. Conventionally, BGR can achieve a good temperature coefficient (TC) when the specific ratio of proportional to absolute temperature (PTAT) current and the complementary to absolute temperature (CTAT) current is attained under certain circumstances. TC is commonly compensated by adjusting the ratio in accordance with the process variation. Unlike the conventional compensation of manual trial with a resistor and a switch array, the mechanism of the proposed BGR without off-chip trimming proposed herein is illustrated in Fig. 9. Under the assumption that the op-amp in BGR is ideal, the main factor influencing BGR is the variation in the resistance value R_1. The correlation is like a V-shaped curve, as shown in the left part of Fig. 9(b), with the x-axis as the resistance value and the y-axis as the TC of BGR. Variations in resistance are suppressed by introducing two compensation units, namely, I_{NL1} and I_{NL2}. Given that a smaller resistance R_1 implies a stronger PTAT current than that of the optimized design, I_{NL1} should provide a high-order CTAT current in low-resistance R_1 situations, whereas I_{NL2} should provide a high-order PTAT current in high-resistance R_1 situations. Compensation is achieved by M_{C1} and M_{C3}, which serve as the current source and sink, respectively. The added or drawn current changes the current density of BJT to restore the optimal ratio of I_{PTAT} and I_{CTAT}. M_{C1} and M_{C3} are operated in subthreshold region for nonlinear compensation, which only generate the compensation current in the desired temperature region and maintain a negligible value in the other temperature regions. For example, the V_{GS} of M_{C1} decreases as temperature increases, resulting in the CTAT characteristics of I_{NL1}. Similarly, the V_{GS} of M_{C4} decreases as temperature increases, thereby creating a PTAT current I_{NL2} through M_{C3}. However, the amount of compensation should change accordingly to cancel out the effects of I_{PTAT} variations whenever the resistor process shifts toward point A or point C from point B. The mechanism is realized by controlling the current source of compensation path. When R_1 increases, the output voltage of the amplifier and V_{B1} also increases, resulting in a decrease in I_{NL1} and an increase in I_{NL2}, as shown in Fig. 9(a). By simply combining these two compensation units, a flat curve of TC after compensation can be obtained throughout the resistor variations in R_1, as shown in the right part of Fig. 9(b).

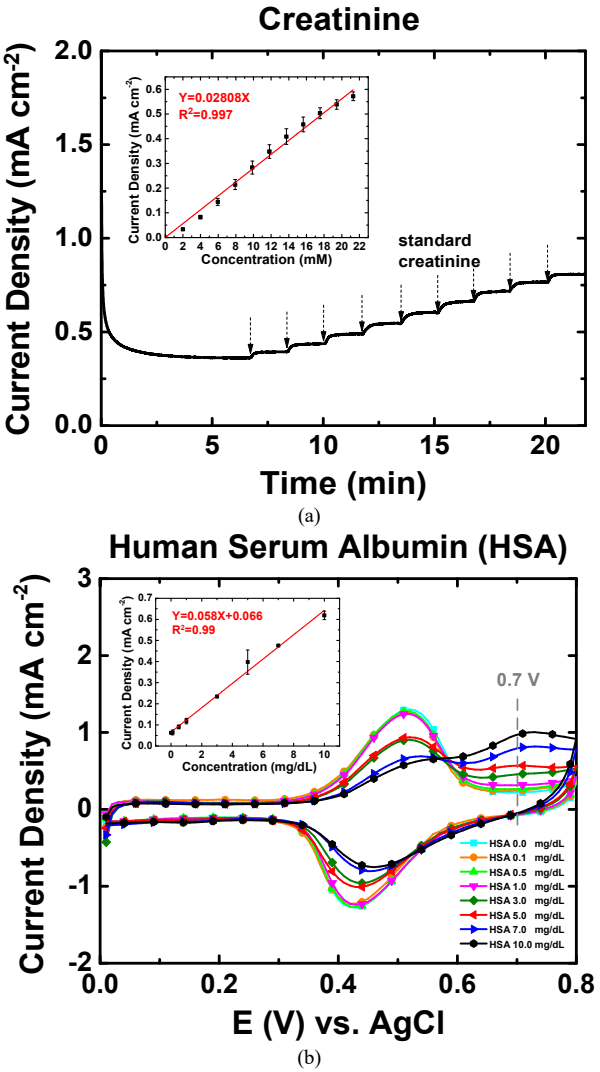

Fig. 10. (a) CA measurement results and (b) CV measurement results of the creatinine and albumin detection.

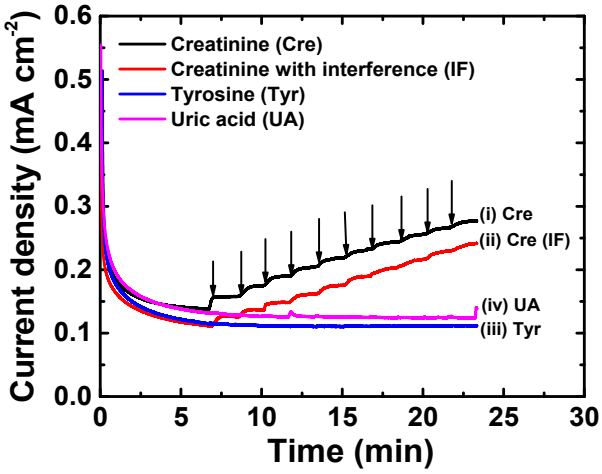

Fig. 11. Measured amperometric responses of the interference minimization for creatinine detection with the Nafion® overlayer in actual urine samples. The curves of successive additions of (i) creatinine without interference, (ii) creatinine with interference, (iii) tyrosine, and (iv) uric acid are all plotted for the comparison.

This article has been accepted for publication in a future issue of this journal, but has not been fully edited. Content may change prior to final publication. Citation information: DOI 10.1109/TBCAS.2021.3087475, IEEE Transactions on Biomedical Circuits and Systems

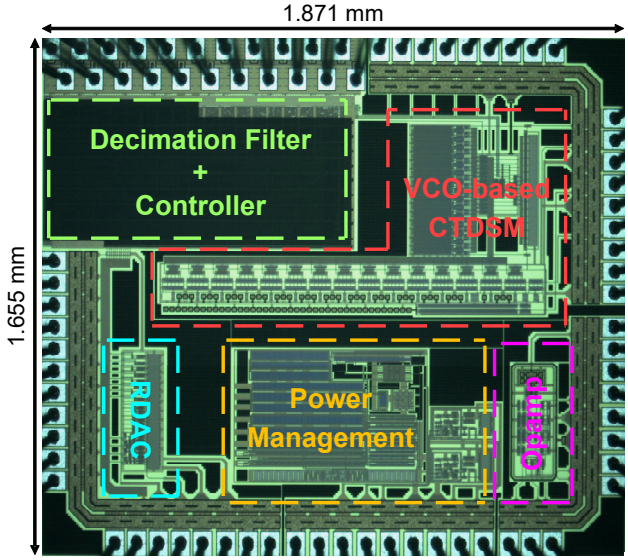

Fig. 12. Microphotograph of the proposed ASIC.

IV. Measurement Results

A. Amperometric Characteristics of ABTS-CNT Biosensor

The results of amperometric tests by CHI 660 on the proposed electrochemical biosensor are shown in Fig. 10. The results of CA experiments for creatinine detection are obtained by stimulation at a fixed potential of 1.05 V to each successive addition of creatinine (Fig. 10(a)). The calibration curve can achieve a coefficient of determination (R^2) of 0.997 compared with the standard concentration tested using a biochemical analyzer (TBA^{TM}-25FR). For HSA detection, CV measurements (Fig. 10(b)) are performed within the potential range of 0–0.8 V after 30 minutes soaking the biosensor in the tested urine. Experiment results show an anodic peak current density at 0.7 V, which increases as HSA concentration increases. The calibration curves of the different HSA concentrations are obtained by each current density at 0.7 V within the range of 0.1–10 mg/dL and can achieve an R^2 value of 0.99.

The interference due to actual urine samples for creatinine detection is minimized by applying a Nafion® overlayer. The amperometric responses of the proposed biosensor to successive additions of (i) creatinine with major interferences in urine, including (iii) tyrosine (Tyr) and (iv) uric acid (UA), are given in Fig. 11. According to the level of normal concentration in urine, each addition for curves (i), (iii), and (iv) is 2, 0.08, and 0.022 mM, respectively. The amperometric response of creatinine increases higher than that of Try and UA. The curve (i) without interfering species and (ii) with interfering species show little difference, suggesting a high selectivity by covering the ABTS-CNT composite with a Nafion® overlayer.

B. ASIC Performance

The proposed electrochemical readout ASIC fabricated in TSMC standard 0.18 µm CMOS process occupies a total chip area of 3.1 mm^2, and a microphotograph labeled with each circuit block is given in Fig. 12. The proposed current-sensing VCO-based 2nd-order CTDSM consumes 580 µW operating at 25.6 kS/s under 1.8 V supply to act as an alternative current readout circuit mentioned in Fig. 3(b). The total power consumption

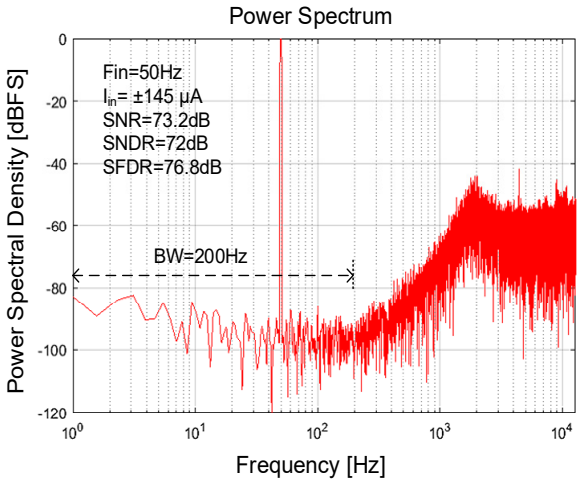

Fig. 13. Power spectral density of the proposed VCO-based CTDSM.

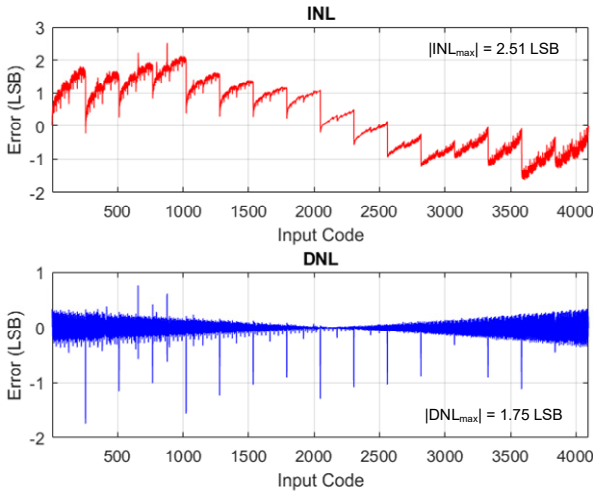

Fig. 14. INL and DNL measurement results of the hybrid R-DAC.

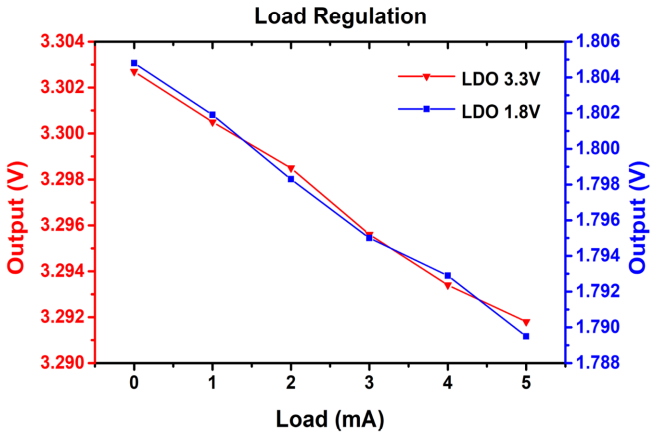

Fig. 15. Load regulation of LDO with 3.3 and 1.8 V outputs.

increases to 595.7 µW at AFE including the decimation filter and the other digital circuitry, leading to a slightly degraded power efficiency of 0.9. The measured power spectrum of the proposed DSM output without demodulation is shown in Fig. 13. The

This article has been accepted for publication in a future issue of this journal, but has not been fully edited. Content may change prior to final publication. Citation information: DOI 10.1109/TBCAS.2021.3087475, IEEE Transactions on Biomedical Circuits and Systems

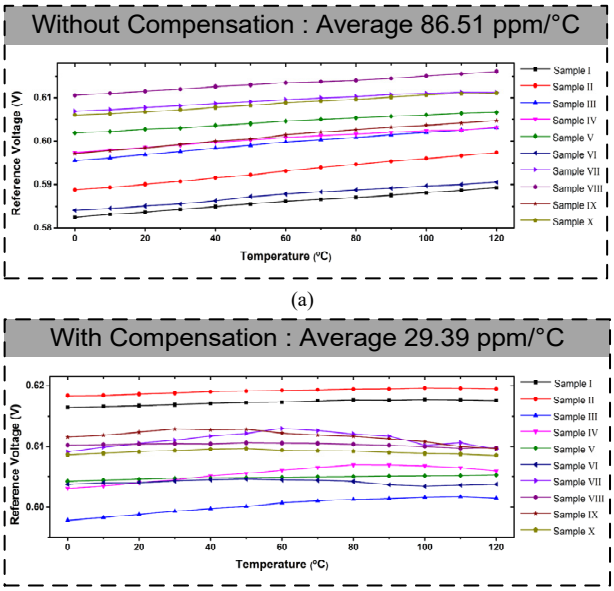

Fig. 16. TC profile of (a) 10 samples without compensation (b) 10 samples with the proposed compensation technique.

input signal is a 50 Hz current sinewave generated by Keithley 6221 with an amplitude of 145 µA, which almost covers the entire input range of the redox reaction current from the proposed electrochemical biosensor. The proposed CTDSM can achieve a peak SNDR of 72 dB, a spurious-free dynamic range (SFDR) of 76.8 dB, and a DR of 75.2 dB. The power efficiency, which is defined in [13] equal to the ratio of input current range to maximum consumed current, can be up to 0.93 without the digital circuitry in this design.

The measurement results of the 12-bit hybrid R-DAC as the pattern generator for potentiostat are given in Fig. 14. The maximum DNL and INL is 1.75 and 2.51 LSB, respectively, where the critical DNL errors always occur at the moment of switching between the 4-bit coarse segment and the 8-bit fine segment. The error tones repeatedly appear per 256 input digital codes. The power consumption of the hybrid R-DAC is approximately 560 µW under 3.3 V supply, where the class-AB output buffer accounts for about 90% because of the driving ability for the sensor loading current and the stability for the uncertain equivalent feedback network in the tested solution.

The measurement result of LDO for the power management of ASIC is shown in Fig. 15. The load regulation of 3.3V and 1.8V LDO within the range of 0–5 mA and at an off-chip capacitor of 0.22 µF is 2.2 and 3.3 mV/mA, respectively. The line regulation of 3.3V is 11.2 mV/V with an input voltage of 4.3–3.7 V from a Li-ion battery, and the line regulation of 1.8V LDO is 5.5 mV/V with an input voltage of 3.4–3.2 V. The quiescent current (I_Q) of the 3.3-V LDO and the 1.8-V LDO is 83 and 78.6 µA, respectively. With the two LDOs, the entire electrochemical system is supplied with clean power. The TC measurement results of BGR with and without the proposed compensation technique are given in Fig. 16. Without any compensation, the average TC of 10 samples is 86.51 ppm/°C, whereas the proposed BGR with the compensation technique against the resistor variation can achieve an average TC of 29.39

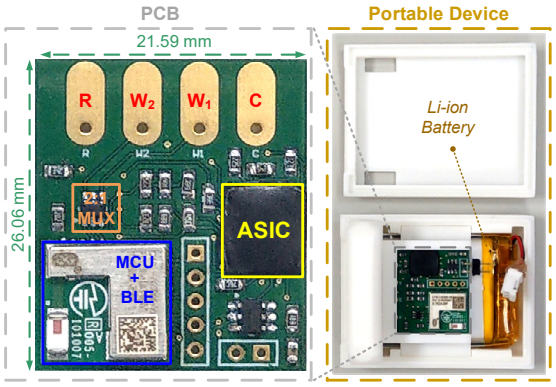

Fig. 17. Photograph of the integrated PCB within a portable device. The circuit block diagram of the PCB is as same as the one shown in Fig. 1.

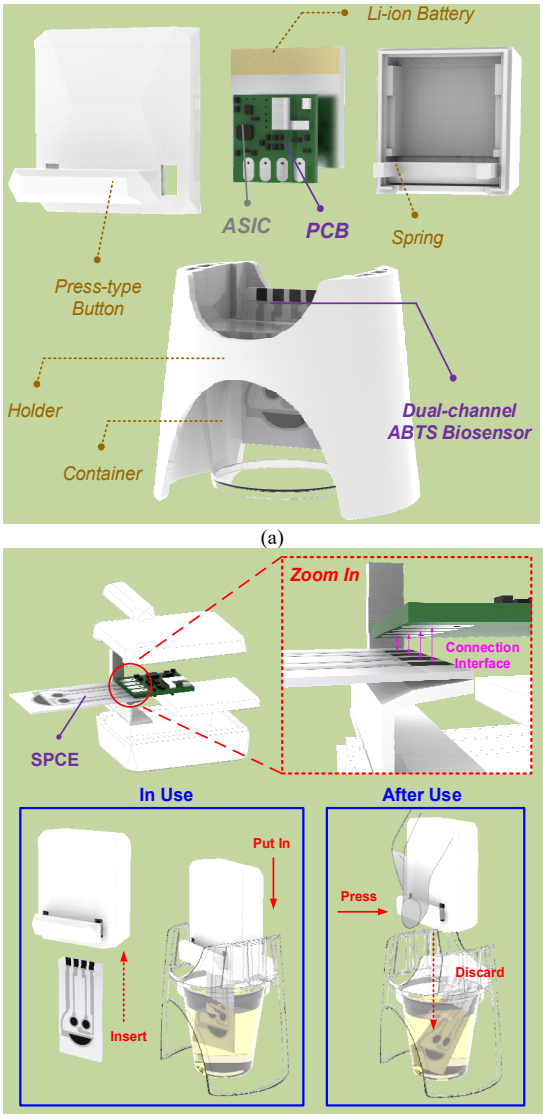

Fig. 18. (a) Exploded view of the prototype for the urine detection system with the integrated PCB and the disposable SPCE. (b) Enlarged view of the connection interface between the SPCE and the portable device with the procedure of the use of prototype.

This article has been accepted for publication in a future issue of this journal, but has not been fully edited. Content may change prior to final publication. Citation information: DOI 10.1109/TBCAS.2021.3087475, IEEE Transactions on Biomedical Circuits and Systems

TABLE I
SUMMARY OF THE DETAILED PERFORMANCE OF ASIC

ASIC Summary			
Tech.	TSMC 0.18 μm 1P6M	Area	1.871 x 1.655 mm^2
Potentiostat @ 1.8V / 3.3V		**Power Management @ 3.7V ~ 4.3V**	
Current-sensing VCO-based 2nd-order CTDSM	F_S = 25.6 kHz Bandwidth = 200 Hz Input Range = ± 150 μA Accuracy = 52 nA SNDR = 72 dB SFDR = 76.8 dB DR[1] = 75.2 dB Power Diss. = 580 μW Power Eff.[2] = 0.93	LDO (1.8V)	Loading Current = 5 mA Line Regulation = 5.5 mV/V Load Regulation = 3.3 mV/mA I_Q = 78.6 μA
		LDO (3.3V)	Loading Current = 5 mA Line Regulation = 11.2 mV/V Load Regulation = 2.2 mV/mA I_Q = 83 μA
Hybrid R-DAC	Output Range = 3.3 V Offset Error = -0.2 μV Gain Error = 0.03265 % DNL_{max} = 1.75 LSB INL_{max} = 2.51 LSB	BGR	Temp. Range = 0~120 °C V_{ref} = 609.3 mV Average TC = 29.39 ppm/°C Best TC = 12.22 ppm/°C PSRR = -40.7 dB @ 1kHz I_Q = 58.3 μA
Digital Circuitry @ 1.8V			
Dec. Filter	Bandwidth = 185 Hz Word Length = 20 bits IMD_3 = 70 dB	UART	Baud Rate = 19200 TX = 3 package/time RX = 2 package/time $F_{operation}$ = 307.2 kHz
Core Power	15.7 μW		

[1] DR = ± Input Range / Accuracy
[2] Power Eff. [13] = ± Input Range / Maximum Consumed Current

ppm/°C within 0 °C–120 °C. The best TC is 12.22 ppm/°C without off-chip trimming. The power supply rejection ratio (PSRR) is −40.7 dB at 1kHz and the current consumption I_Q is 58.3 μA, which can provide a reference voltage of about 0.6 V.

The other detailed performances of each circuit block in the proposed ASIC are summarized in Table I. This work presents a power-efficient electrochemical readout ASIC for the proposed urine detection system, which consists of the required peripherals that are integrated in a printed circuit board (PCB).

C. Experiments of Urine Tests

A photograph of the integrated PCB within a portable device is given in Fig. 17. It mainly contains the proposed ASIC, an MCU with the Bluetooth module, and a single-pole-double-throw switch with a 4-pin connector interface connected to the dual-channel SPCE. The PCB has an area of 26.06 mm × 21.59 mm and can be placed into the portable device with a Li-ion battery. The prototype that can be used as a portable wireless urine detector for UACR detection is shown in Fig. 18. This prototype is made of an ultraviolet curable resin with a stereo lithography appearance, and the mechanism of the prototype is designed as a press-button type to make it convenient to use, as shown in Fig. 18(a). Fig. 18(b) shows an enlarged view of the connection interface between the SPCE and the portable device shown in Fig. 17, and the procedure of the use of prototype has also been illustrated as the practical experiment setups. The disposable SPCE can be simply aborted after one use and make a quick replacement for the next use.

The National Cheng Kung University Hospital Institutional Review Board approved this research (IRB No. A-ER-106-421), and all of the patients enrolled gave their informed consent to participate the clinical trial. The experimental environment setup for testing actual urine samples by using the proposed urine

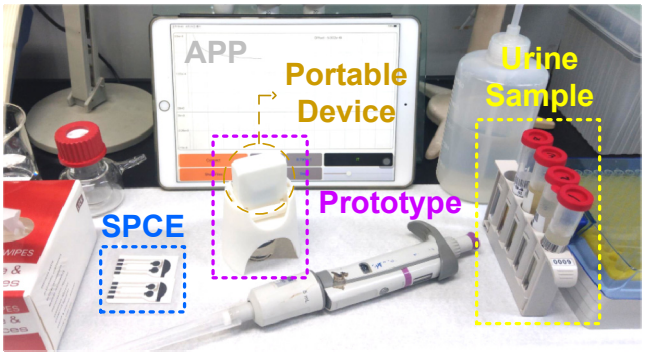

Fig. 19. Experimental environment setup for testing practical urine samples by using the system proposed herein.

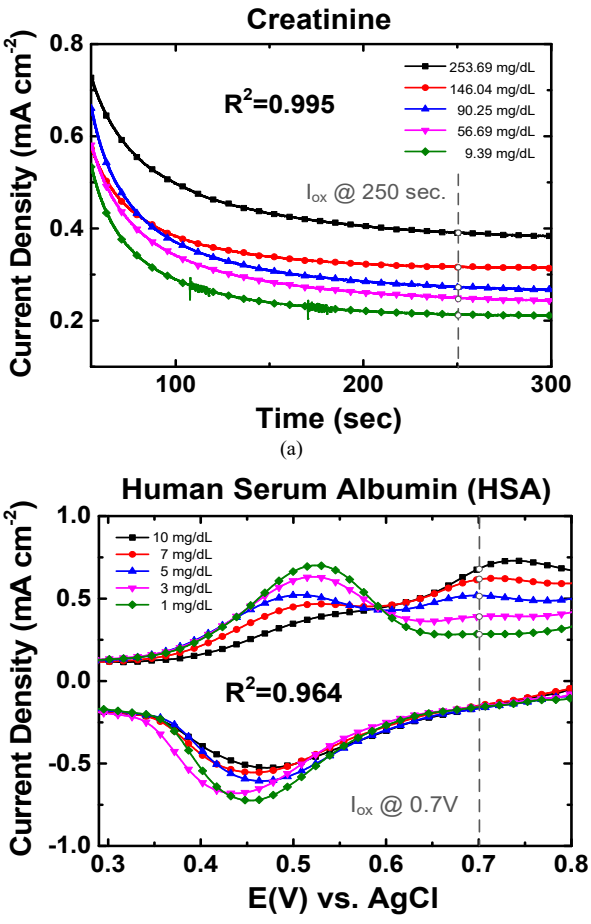

Fig. 20. Experiment results of (a) CA measurement for creatinine detection (b) CV measurement for albumin detection under practical urine tests.

detection system is illustrated in Fig. 19. The proposed electrochemical system is used to test several clinical urine samples for creatinine and HSA detection. Via the SPCE and the portable device, the redox reaction current signal sensed by the ASIC is displayed on the APP developed herein in real-time. The measurement results of the two biomarkers via CA and CV are shown in Fig. 20. The oxidation currents are calculated into their corresponding calibration curves, where each value of R^2 is

TABLE II
PERFORMANCE OF THE URINE DETECTION SYSTEM RELATIVE TO THAT OF OTHER STATE-OF-THE-ART SYSTEMS

Publication	**This Work**	TBCAS'17 [18]	TBCAS'17 [19]	TBCAS'19 [20]
Subject	**Creatinine / Albumin**	Glucose	pH	Potassium Ferricyanide
Tech. (nm)	**180+COTS[1]**	350+COTS[1]	350	180
Chip Size (mm^2)	**3.1[2]**	0.6	0.5	0.78
Electrode Material	**SPCE|ABTS-CNT|Nafion®**	Pt-nanoS	Ag/AgCl	Gold
Electrochemistry	**CA/CV**	CA/CV	-	CA/CV
Supply (V)	**3.3 / 1.8**	3.3	1.5	1.2
Input Range	**± 150 µA**	± 20 µA	0.2 µA ~ 3 µA	± 5 µA
Accuracy	**52 nA**	0.47 pA	0.1 nA	41 pA
Dynamic Range	**75.2 dB**	156 dB[3]	88.9 dB	108 dB
Power Diss.[4]	**595.7 µW**	6.57 mW[5]	16.8 µW	16 µW
Power Eff.[4]	**0.9**	0.02[5]	0.25	0.75
Total Chip Power	**1.85 mW[6]**	9.3 mW	16.8 µW	16 µW
On-Chip Pattern Gen.	**Yes**	Yes	No	Yes
Signal Processing	**Cortex-M0**	tinyAVR	-	-
Communication Protocol	**UART**	SPI	-	-
Prototype	**Yes**	-	-	-
User Interface	**APP**	-	-	-

[1] The MCU and Bluetooth are off-chip combined in the system.
[2] Total chip area instead of active area only.
[3] Dynamic range across multiple gain settings.
[4] Calculated only based on the readout circuit. Power Eff. [13] = ± Input Range / Maximum Consumed Current
[5] For fair comparison, the power dissipation of DAC has been omitted from given information.
[6] Including the potentiostat, digital circuitry, and power management circuit.

equal to 0.995 and 0.964 compared with the standard measurement results tested by TBA™-25FR. The experiment results demonstrate the capability of the urine detection system for UACR detection. Hence, this system can provide not only an accurate measurement for biomedical analysis but also a useful system platform for commercial applications. The performance of the system relative to that of other state-of-the-art systems in terms of electrochemical readout is provided in Table II. The system proposed herein has a high power efficiency because of the proposed electrochemical readout ASIC.

V. CONCLUSION

This work presented a portable wireless urine detection system and a platform for UACR detection based on the proposed electrochemical readout ASIC and the ABTS-CNT biosensor. The ASIC fabricated in TSMC 0.18 µm CMOS process consists of a current-sensing VCO-based 2nd-order CT delta-sigma ADC and a hybrid R-DAC as the potentiostat at AFE to be able to perform electrochemical detection. The delta-sigma ADC can achieve a wide DR of 75.2 dB with a high power efficiency of 0.9 and the hybrid R-DAC has a maximum DNL/INL of 1.75/2.51 LSB, respectively. The electrochemical ABTS-CNT biosensor with high sensitivity and selectivity to creatinine and albumin proposed herein uses a Nafion® overlayer to minimize the interference from actual urine samples. A customized prototype was fabricated. Experimental results demonstrated the capability of the proposed urine detection system and suggested that it is suitable for either personal health administration or homecare. Owing to the user-friendliness and convenience of the proposed urine detector, it can help to increase the willingness of users to adopt it, which is helpful for the early detection of cardiovascular risk factors.

ACKNOWLEDGMENTS

The authors highly appreciate the support from the Taiwan Semiconductor Research Institute and the Ministry of Science and Technology, Taiwan (Grants MOST 109-2218-E-006-022 and MOST 109-2622-8-006-021-TE2).

REFERENCES

[1] World Health Organization, "Cardiovascular diseases (CVDs)," May 17, 2017. Accessed: May 18, 2020. [Online]. Available: https://www.who.int/en/news-room/fact-sheets/detail/cardiovascular-diseases-(cvds).

[2] K. Matsushita, J. Coresh, Y. Sang, J. Chalmers, C. Fox, E. Guallar, et al., "Estimated glomerular filtration rate and albuminuria for prediction of cardiovascular outcomes: a collaborative meta-analysis of individual participant data," *Lancet Diabetes & Endocrinology*, vol. 3, no.7, pp. 514-525, July 2015.

[3] U. Lad, S. Khokhar and G. M. Kale, "Electrochemical Creatinine Biosensors," *Anal. Chem,* 2008, 80, 21, 7910-7917.

[4] D. F. Putnam, "Composition and concentrative properties of human urine," *NASA Contractor Reports*, 1971, NASA-CR-1802.

[5] R. T. Lagua and V. S. Claudio, "Nutrition and Diet Therapy Reference Dictionary," *4 ed. Springer Netherlands*, 1996, p. 491.

[6] H. J. Lambers Heerspink et al., "Albuminuria Assessed From First-Morning-Void Urine Samples Versus 24-Hour Urine Collections as a Predictor of Cardiovascular Morbidity and Mortality," *American Journal of Epidemiology*, vol. 168, no. 8, pp. 897-905, 2008.

[7] A. Sun, A. G. Venkatesh and D. A. Hall, "A Multi-Technique Reconfigurable Electrochemical Biosensor: Enabling Personal Health Monitoring in Mobile Devices," *IEEE Trans. Biomed. Circuits Syst.*, vol. 10, no. 5, pp. 945-954, Oct. 2016.

[8] B. Nasri et al., "Hybrid CMOS-Graphene Sensor Array for Subsecond Dopamine Detection," *IEEE Trans. Biomed. Circuits Syst.*, vol. 11, no. 6, pp. 1192-1203, Dec. 2017.

[9] F. Stradolini et al., "An IoT Solution for Online Monitoring of Anesthetics in Human Serum Based on an Integrated Fluidic Bioelectronic System," *IEEE Trans. Biomed. Circuits Syst.*, vol. 12, no. 5, pp. 1056-1064, Oct. 2018.

[10] D. S. Ciou, P. H. Wu, Y. C. Huang, M. C. Yang, S. Y. Lee and C. Y. Lin, "Colorimetric and amperometric detection of urine creatinine based on the ABTS radical cation modified electrode," *Sensors and Actuators B: Chemical*, vol. 314, pp.128034, July 2020.

[11] C. Tu, Y. Wang and T. Lin, "A Low-Noise Area-Efficient Chopped VCO-Based CTDSM for Sensor Applications in 40-nm CMOS," *IEEE J. Solid-State Circuits*, vol. 52, no. 10, pp. 2523-2532, Oct. 2017.

[12] H. Y. Lee, P. W. Huang, D. S. Ciou, Z. X. Liao and S. Y. Lee, "A Power-Efficient Current Readout Circuit with VCO-Based 2nd-Order CT ΔΣ ADC for Electrochemistry Acquisition," *IEEE Asian Solid-State Circuits Conf. (A-SSCC)*, Hiroshima, Japan, 2020, pp. 1-2.

[13] H. Li, C. S. Boling and A. J. Mason, "CMOS amperometric ADC With high sensitivity, dynamic range and power efficiency for air quality monitoring," *IEEE Trans. Biomed. Circuits Syst.*, vol. 10, no. 4, pp. 817–827, Aug. 2016.

[14] P. Prabha et al., "A Highly Digital VCO-Based ADC Architecture for Current Sensing Applications," *IEEE J. Solid-State Circuits*, vol. 50, no. 8, pp. 1785-1795, Aug. 2015.

[15] H. Jeon, J. Bang, Y. Jung, I. Choi and M. Je, "A High DR, DC-Coupled, Time-Based Neural-Recording IC With Degeneration R-DAC for Bidirectional Neural Interface," *IEEE J. Solid-State Circuits*, vol. 54, no. 10, pp. 2658-2670, Oct. 2019.

[16] S. Y. Lee, P. W. Huang, J. R. Chiou, C. Tsou, Y. Y. Liao and J. Y. Chen, "Electrocardiogram and Phonocardiogram Monitoring System for Cardiac Auscultation," *IEEE Trans. Biomed. Circuits Syst.*, vol. 13, no. 6, pp. 1471-1482, Dec. 2019.

[17] Maxim Integrated. *Determining Clock Accuracy Requirements for UART Communications*. (2003). [Online]. Available: http://www.eecs.umich.edu/courses/eecs373.w05/lecture/AN2141.pdf

[18] S. S. Ghoreishizadeh, I. Taurino, G. De Micheli, S. Carrara and P. Georgiou, "A Differential Electrochemical Readout ASIC With Heterogeneous Integration of Bio-Nano Sensors for Amperometric

Sensing," *IEEE Trans. Biomed. Circuits Syst.*, vol. 11, no. 5, pp. 1148-1159, Oct. 2017.

[19] H. Son et al., "A Low-Power Wide Dynamic-Range Current Readout Circuit for Ion-Sensitive FET Sensors," *IEEE Trans. Biomed. Circuits Syst.*, vol. 11, no. 3, pp. 523-533, June 2017.

[20] Y. C. Chen, S. Y. Lu and Y. T. Liao, "A Microwatt Dual-Mode Electrochemical Sensing Current Readout With Current-Reducer Ramp Waveform Generation," *IEEE Trans. Biomed. Circuits Syst.*, vol. 13, no. 6, pp. 1163-1174, Dec. 2019.

Shuenn-Yuh Lee (M'98-SM'15) was born in Taichung, Taiwan, in 1966. He received the B.S. degree from the National Taiwan Ocean University, Keelung, Taiwan, in 1988, and the M.S. and Ph.D. degrees from the National Cheng Kung University, Tainan, Taiwan, in 1994 and 1999, respectively.
He is currently a Professor at the Department of Electrical Engineering, National Cheng Kung University, Tainan, Taiwan. He served as the Technical Program Chair (TPC) of the 2014/2015 International Symposium on Bioelectronics & Bioinformatics (ISBB), and the 2015 Taiwan and Japan Conference on Circuits and Systems (TJCAS). From 2013 to 2016, he serves as the Chairman of IEEE Solid-State Circuits Society Tainan Chapter. From 2016 to 2017, he serves as the Vice Chairman of IEEE Tainan Section. From 2016, he serves as the Associate Editor of IEEE Transaction on Biomedical Circuits and Systems.
His present research activities involve the design of analog and mixed-signal integrated circuits, biomedical circuits and systems, low-power and low-voltage analog circuits, and RF front-end integrated circuits for wireless communications. Dr. Lee now is a member of Circuits and Systems (CAS) Society, Solid-State Circuits Society, and Medicine and Biology Society of IEEE. He is also a member of IEICE.

Hao-Yun Lee was born in Taipei City, Taiwan, R.O.C., in 1994. He received the B.S. degree from National Cheng Kung University, Tainan, Taiwan, R.O.C., in 2017.
He is currently pursuing Ph.D. degree with Department of Electrical Engineering, National Cheng Kung University, Taiwan. His research interests include the design of analog front-end circuit, analog/mixed-signal integrated circuits, and biomedical implantable systems.

Ding-Siang Ciou was born in Kaohsiung, Taiwan, in 1992. He received his B.S. degree in Electrical Engineering from National Cheng Kung University, Taiwan, in 2016. Currently, he is a PhD student in Electrical Engineering, National Cheng Kung University under supervision of Prof. Shuenn-Yuh Lee.
His researches focused on electrochemical sensors, sensing devices, biomedical circuits and systems development.

Zhan-Xian Liao was born in Kaohsiung, Taiwan, in 1995. He received the B.S. degree from the National Cheng Kung University, Taiwan, in 2017.
He is currently pursuing Ph.D. degree with Department of Electrical Engineering, National Cheng Kung University, Taiwan. His research interests include power management IC design.

Peng-Wei Huang (S'19) was born in Tainan, Taiwan, R.O.C., in 1990. He received the B.S. degree from National Cheng Kung University, Taiwan, in 2013. He is currently pursuing the Ph.D. degree from the Institute of Electrical Engineering, National Cheng Kung University, Tainan, Taiwan.
His research interests include the design of digital integrated circuits, software development, and biomedical circuits and systems.
His awards and accepted papers include excellent work in 2014 cell-based digital circuit design hold by CIC, Taiwan, excellent work in 2015 Silicon Awards held by Macronix, Taiwan, and attended 2015 ISBB.

Yi-Ting Hsieh was born in Kaohsiung City, Taiwan, R.O.C., in 1997. He received the B.S. degree from National Cheng Kung University, Tainan, Taiwan, R.O.C., in 2019.
He is currently pursuing Ph.D. degree with Department of Electrical Engineering, National Cheng Kung University, Taiwan. His research includes analog front-end circuit, analog/mixed-signal integrated circuits, digital signal processing and biomedical implantable systems.

Yi-Chieh Wei was born in Taipei City, Taiwan, R.O.C., in 1991. He received the bachelor degree in industrial design from National Cheng Kung University, Tainan, Taiwan, R.O.C., in 2016.
He is currently pursuing master's degree with Department of Industrial Design, National Cheng Kung University, Taiwan. His research interests include the medical product design and development, assistive technology in elderly care, and mold of plastics.

Chia-Yu Lin received his B.S. degree in Chemical Engineering from National Cheng Kung University, Taiwan, in 2003. He received his M.S. and Ph.D. degrees in Chemical Engineering from National Taiwan University, Taiwan in 2005 and 2010, respectively. After two-year postdoctoral research in Department of Chemistry, University of Cambridge, United Kingdom, he joined the Department of Chemical Engineering, National Cheng Kung University, Taiwan, in 2013. Currently, he is an Associate Professor in Department of Chemical Engineering, National Cheng Kung University, Taiwan.
His researches mainly focused on Electrochemical Engineering for chemical sensors, (photo-)electrocatalysis, and energy-conversion devices.

Meng-Dar Shieh, Professor, Department of Industrial Design, National Cheng Kung University, Tainan, Taiwan. He got his Ph.D. (1990) and M.S. degrees (1986) in Mechanical Engineering, University of Florida, USA.
His research interests include Neural Network, Kansei Engineering, Artificial Intelligence, Concurrent Engineering, Computer Graphics Simulation, Virtual Reality, Computer-Aided Design and Manufacturing, Product Design, System Integration and Networking, Robotics in Medical Applications, Quality Control, Digital Design, E-commerce.

Ju-Yi Chen was born in Tainan, Taiwan, in 1974. He received the M.S. degree from the Chang Gung University, Taoyuan City, Taiwan, in 1999, and the Ph.D. degrees from the National Cheng Kung University, Tainan, Taiwan, in 2013.

He is currently an Associate Professor from 2013, at the Department of Internal Medicine, National Cheng Kung University, Tainan, Taiwan.

His present research activities involve the cardiovascular diseases, including arrhythmias, hypertension, arterial stiffness, and cardiac implantable electric devices.